Influence of IGBT and Diode Parameters on the Current Sharing and Switching-Waveform Characteristics of Parallel-Connected Power Modules

Y. Ando*, J. Sakai, K. Hatori
Mitsubishi Electric Corporation
1-1-1, Imajukuhigashi Nishi-ku
Fukuoka 819-0192, Japan
Tel.: +81 – 92 – 805 – 4251
Fax: +81 – 92 – 805 – 3676
*E-Mail: Ando.Yu@bx.MitsubishiElectric.co.jp
URL: http://www.MitsubishiElectric.com

N. Soltau, E. Wiesner*
Mitsubishi Electric Europe B.V.
Mitsubishi-Electric-Platz 1,
40882 Ratingen, Germany
Tel.: +49 2102 486 0
Fax: +49 2102 486 7220
*E-Mail: Eugen.Wiesner@meg.mee.com
URL: http://www.Mitsubishichips.eu

Keywords

«Power semiconductor device», «Paralleling», «Parallel operation», «Device characterization», «Current balancing»

Abstract

The parallel connection of IGBT power modules allows flexible power converter designs. However, differences in parameters like forward and threshold voltage (ΔV_{CEsat}, $\Delta V_{GE(th)}$, and ΔV_{EC}) between parallel-connected power modules may particularly influence static and dynamic current sharing, and switching characteristics, among several factors. Therefore, when designing converters with parallel-connected power modules, current sharing and switching characteristics of individual power modules must be considered to ensure operation within safe operating area and temperature limits. Derating is to be considered if necessary. Identifying the influential parameters in a parallel-connection, and quantifying their influence on current sharing and switching characteristics, are essential to understand and optimize the amount of derating. This paper first describes the measurement results of ten parallel-connected pairs of 3.3 kV IGBT power modules. Afterwards, the imbalance of switching characteristics (such as switching energy or current amount) is related to power-module parameters, by multiple linear regression. Fanally a methodology for defining the derating ratio for each switching characteristic is described.

Introduction

In many applications, the parallel connection of IGBT power modules allows more flexible power converter designs due to the scalability of converter output power. In the railway application, for example, this topic is discussed in the Horizon 2020 Project “Roll2Rail” [1].
The main challenge in parallel connecting IGBT power modules is homogeneous current sharing among parallel connected devices. The current sharing must be considered during the conduction and switching of the devices respectively [2][3]. For this, special power modules for simplified parallel connection have become available, as well as setup for the characterization [4][5][6].
However, homogenous current sharing remains challenging as it is strongly influenced by power-module parameters and the converter design. Besides dedicated and deliberate converter design, proper selection of power modules by its parameters is required.
This paper analyses the influence of parameter differences of parallel-connected power modules on current sharing and switching energies. Firstly, the test method, devices under test, and test setup are introduced briefly. After that, multiple regression analysis is performed on the measurement results to identify highly influential parameters. Finally, these parameters are used to calculate the derating ratio for each characteristic and define the selection criteria for devices used for parallel connection.

Methodology

This paper analyzes the influence of different IGBT power module parameters, i.e. collector-emitter saturation voltage V_{CEsat}, gate-emitter threshold voltage $V_{GE(th)}$, and diode forward voltage V_{EC}, on switching-waveform characteristics of parallel-connected power modules. For this, IGBT turn-off, IGBT turn-on, and diode turn-off (reverse recovery) have been measured with ten parallel-connected pairs of power modules, respectively. Each pair has a unique value in terms of the differences of power module parameters (ΔV_{CEsat}, $\Delta V_{GE(th)}$, and ΔV_{EC}). Switching characteristics, i.e. switching current or switching energies, are derived from each measurement and related to the differences in parameters of each pair. Then, via multiple regression analysis, the highly influential parameters are identified for each switching characteristic. Afterwards, formulas are defined for the imbalance ratio of each characteristic and its prediction interval.

Devices under Test and Test Setup

The devices under test are MITSUBISHI ELECTRIC 3.3 kV IGBT power modules with a current rating of 450 A, as shown in Figure 1. Power modules use the LV100 package [6]. Ten pairs of these devices are measured in parallel connections of two modules. The devices have been selected to get a wide distribution of parameter differences between pairs. Table I shows the parameters of individual power modules and the parameter differences between them when paired. The parameter differences are calculated for power module A-power module B.

Table I: Parameters of Devices under Test and Parameter Difference of Pairs

	Power Module A			Power Module B			Pair A-B		
Parameter	V_{CEsat}	$V_{GE(th)}$	V_{EC}	V_{CEsat}	$V_{GE(th)}$	V_{EC}	ΔV_{CEsat}	$\Delta V_{GE(th)}$	ΔV_{EC}
Conditions / Pair No.	I_C=450A, T_j=150°C	I_C=45mA, V_{CE}=10V, T_j=25°C	I_E=450A, V_{GE}=0V, T_j=150°C	I_C=450A, T_j=150°C	I_C=45mA, V_{CE}=10V, T_j=25°C	I_E=450A, V_{GE}=0V, T_j=150°C	I_C=450A, T_j=150°C	I_C=45mA, V_{CE}=10V, T_j=25°C	I_E=450A, V_{GE}=0V, T_j=150°C
1	2.70 V	6.57 V	2.20 V	2.72 V	6.57 V	2.22 V	-0.02 V	0.00 V	-0.02 V
2	2.70 V	6.57 V	2.20 V	2.63 V	7.70 V	2.34 V	0.07 V	-0.51 V	-0.14 V
3	2.61 V	6.98 V	2.43 V	2.81 V	7.53 V	2.37 V	-0.20 V	-0.54 V	0.06 V
4	2.61 V	6.98 V	2.43 V	2.70 V	6.57 V	2.20 V	-0.09 V	0.42 V	0.23 V
5	2.70 V	6.57 V	2.20 V	2.72 V	7.25 V	2.45 V	-0.02 V	-0.68 V	-0.26 V
6	2.64 V	6.97 V	2.45 V	2.64 V	6.94 V	2.25 V	0.00 V	0.03 V	0.20 V
7	2.64 V	6.97 V	2.45 V	2.67 V	6.97 V	2.35 V	-0.03 V	0.00 V	0.10 V
8	2.81 V	7.53 V	2.37 V	2.67 V	6.56 V	2.35 V	0.14 V	0.97 V	0.02 V
9	2.63 V	6.95 V	2.45 V	2.64 V	6.97 V	2.45 V	-0.01 V	-0.02 V	0.00 V
10	2.81 V	7.53 V	2.37 V	2.63 V	7.07 V	2.34 V	0.17 V	0.45 V	0.03 V

As mentioned in the introduction, the key requirement from the railway market for these new packages is scalability. It allows converter manufacturers to have flexibility in different projects to design the required output power. For example, by using the one, two or six CM450DA-66X modules, the current ratings of 450 A, 900 A or 2700 A can be achieved respectively.
The power modules in parallel connection must be operated properly, but since different converter manufacturers have different designs, railway manufacturers agreed on the reference test setup for the evaluation of parallel connections [5]. This reference setup, as depicted in Figure 2, allows evaluation of up to six paralleled modules. The reference test setup was designed to minimize the influence of external factors on the parallel connection. Each power module is connected to a DC-link capacitor with symmetrical and equivalent stray inductance. Furthermore, the gate driver connection should have a symmetrical connection from the gate driver to each parallel-connected power module. The benefit of using this reference test setup is that the user can reproduce the results presented here because the components used, such as gate driver, DC-link capacitors, current probes, and their geometries are standardized. The reference test setup shown in Figure 2 was used to evaluate the ten pairs of power modules shown in Table I. In this evaluation, only two module positions No. 3 and No. 4 with two DC-Link capacitors were used.

Fig. 1: MITSUBISHI ELECTRIC 3.3 kV IGBT power module using the LV100 package [6]

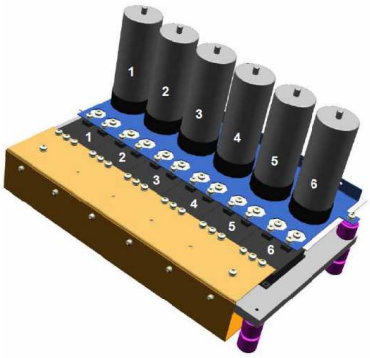

Fig. 2: Reference test setup for LV100 device evaluation [5]

Results

For each pair, IGBT turn-off, IGBT turn-on and diode reverse recovery have been measured under the following conditions, respectively: DC-link voltage V_{CC} = 1800 V, target collector current I_C = 450 A/module, junction temperature T_j = 150°C, DC-link inductance L_s = 65 nH/module, gate voltage V_{GE} = +15 V / -10 V, turn-on and turn-off gate resistance $R_{G(on)}$ = 3.0 Ω/module and $R_{G(off)}$ = 51 Ω/module. Examples of waveforms for each measurement are shown in Figure 3, Figure 4 and Figure 5.

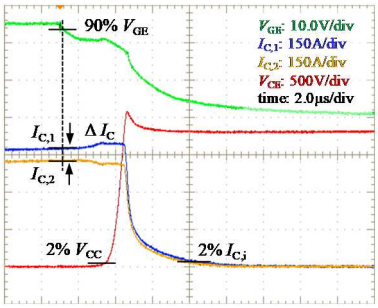

Fig. 3: Exemplary turn-off waveform with indication of characteristic values

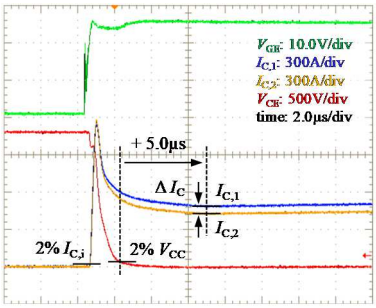

Fig. 4: Exemplary turn-on waveform with indication of characteristic values

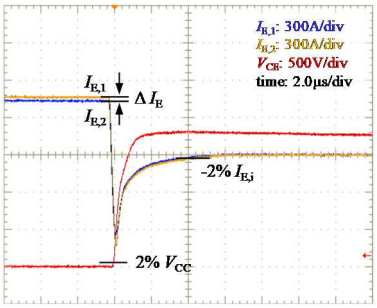

Fig. 5: Exemplary reverse recovery waveform with indication of characteristic values

Regarding IGBT turn-off switching

The turn-off collector currents $I_{C,i}$ (cf. Figure 3) and turn-off energy

$$E_{\mathrm{off},i} = \int_{t(v_{CE}=2\%V_{CC})}^{t(i_{C,i}=2\%I_{C,i})} i_{C,i} \cdot v_{CE}\, \mathrm{d}t \qquad (1)$$

had been evaluated. The index $i \in \{1,2\}$ refers to the individual power modules in the parallel connection.

Table II shows the switching characteristics of individual power modules obtained from the measurements and the pair imbalance ratio calculated based on them. ΔI_C and ΔE_{off} are calculated for power module A-power module B, respectively.

Table II: Switching Characteristics of Each Power Module and Pair Imbalance Ratio in Turn-off Measurements

	Power Module A		Power Module B		Imbalance Ratio	
Pair No.	$I_{C,1}$	$E_{off,1}$	$I_{C,2}$	$E_{off,2}$	x_{I_C}= 0.5 $\Delta I_C/I_{C,avg}$	$x_{E_{off}}$= 0.5 $\Delta E_{off}/E_{off,avg}$
1	447 A	447 A	0.86 J	0.86 J	0.0 %	0.2 %
2	438 A	462 A	0.89 J	0.94 J	-2.7 %	-2.6 %
3	474 A	424 A	1.02 J	0.82 J	5.6 %	10.8 %
4	463 A	437 A	0.95 J	0.90 J	2.9 %	2.9 %
5	451 A	448 A	0.91 J	0.87 J	0.4 %	2.2 %
6	446 A	452 A	0.94 J	0.98 J	-0.7 %	-2.1 %
7	453 A	446 A	0.96 J	0.94 J	0.7 %	1.1 %
8	434 A	463 A	0.81 J	1.00 J	-3.3 %	-10.6 %
9	449 A	455 A	0.96 J	0.98 J	-0.7 %	-1.1 %
10	429 A	471 A	0.82 J	1.02 J	-4.7 %	-10.9 %

Multiple regression analysis has been performed on the power module parameter differences in Table I for each pair and the imbalance ratio in Table II. The power module parameters affecting each switching characteristic were identified.
Figure 6 shows the turn-off collector current imbalance ratio of 0.5 $\Delta I_C/I_{C,avg}$=($I_{C,1}$-$I_{C,2}$)/($I_{C,1}$+$I_{C,2}$), which depends on the collector-emitter saturation voltage differences ΔV_{CEsat}=$V_{CEsat,1}$-$V_{CEsat,2}$ only. By linear regression analysis [7], the measured results can be defined as regression equation (2).

$$x_{I_C\_typ} = 0.5\,\Delta I_C/I_{C,avg} \approx -0.28\ \mathrm{V}^{-1} \cdot \Delta V_{CEsat} \qquad \text{with } R^2 = 0.969 \qquad (2)$$

R^2 is the correlation coefficient, and Figure 7 shows the correlation of the imbalance ratio between the measured results and the calculated results using the regression equation (2). The closer the correlation coefficient R^2 is to 1, the regression equation (2) is the more reliable.
The green line in Figure 7 is the 99% prediction interval (PI=99%). It is given to quantify the accuracy of the regression line, and defined by the following equation.

$$x_{I_C\_PI=99\%} = x_{I_C\_typ} \pm 3.69 \times \sqrt{2.76 \times 10^{-5} \times \left(1 + \frac{1}{10} + \frac{(\Delta V_{CEsat} - 0.002\ \mathrm{V})^2}{0.103\ \mathrm{V}^2}\right)} \qquad (3)$$

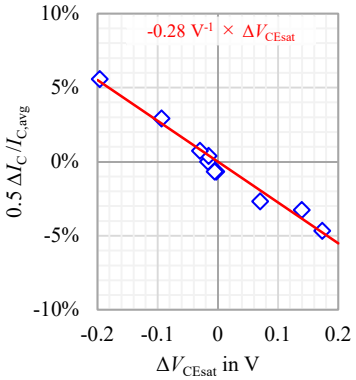

Fig. 6: Imbalance ratio of turn-off current x_{I_C} in dependence of ΔV_{CEsat}

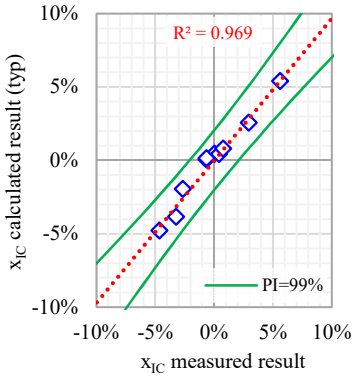

Fig. 7: Correlation of x_{I_C} between calculated and measured results

Differently, the measured results of the imbalance ratios of the turn-off energy 0.5 $\Delta E_{off}/E_{off,avg}$=($E_{off,1}$-$E_{off,2}$)/($E_{off,1}$+$E_{off,2}$) cannot be described satisfactorily in dependence on one parameter only. Instead, it is defined as in regression equation (4) considering both ΔV_{CEsat} and $\Delta V_{GE(th)}$.

$$x_{E_{off}\_typ} = 0.5\,\frac{\Delta E_{off}}{E_{off,avg}} \approx -0.50\ \mathrm{V}^{-1} \cdot \Delta V_{CEsat} - 0.03\ \mathrm{V}^{-1} \cdot \Delta V_{GE(th)} - 0.009 \qquad \text{with } R^2 = 0.993 \qquad (4)$$

Figures 8 and 9 show the imbalance ratios of the turn-off energy $0.5\,\Delta E_{off}/E_{off,avg}=(E_{off,1}-E_{off,2})/(E_{off,1}+E_{off,2})$ that depend on the collector-emitter saturation voltage differences $\Delta V_{CEsat}=V_{CEsat,1}-V_{CEsat,2}$ and the gate-emitter threshold voltage differences $\Delta V_{GE(th)}=V_{GE(th),1}-V_{GE(th),2}$, respectively. Figure 8 includes the intercept of a regression equation (4).
The equation for the 99% prediction interval shown in Figure 10 is defined as (5).

$$x_{E_{off}\_PI=99\%} = x_{E_{off}\_typ} \pm 4.03 \times \sqrt{3.57 \times 10^{-5} \times \left(1 + \frac{1}{10} + \frac{(\Delta V_{CEsat} - 0.002\,V)^2}{0.103\,V^2} + \frac{\left(\Delta V_{GE(th)} - 0.012\,V\right)^2}{2.331\,V^2}\right)} \quad (5)$$

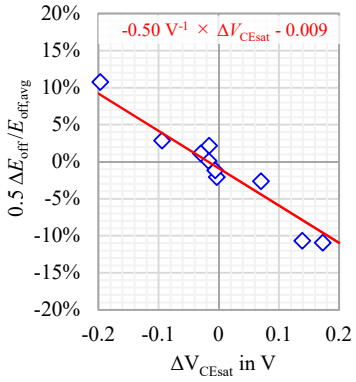

Fig. 8: Imbalance ratio of turn-off energy ($x_{E_{off}}$) in dependence of ΔV_{CEsat}

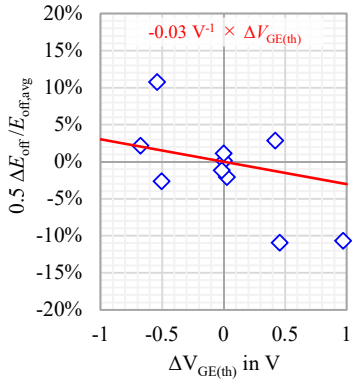

Fig. 9: Imbalance ratio of turn-off energy ($x_{E_{off}}$) in dependence of $\Delta V_{GE(th)}$

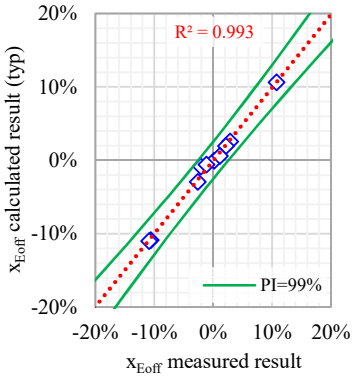

Fig. 10: Correlation of $x_{E_{off}}$ between calculated and measured results

Regarding IGBT Turn-on Switching

The turn-on collector current $I_{C,i}$ (cf. Figure 4) (6) and turn-on energy $E_{on,i}$ (7) have been evaluated.

$$I_{C,i} = i_{C,i}(t(v_{CE} = 2\%V_{CC}) + 5\mu s) \quad (6)$$

$$E_{on,i} = \int_{t(i_{C,i}=2\%I_{C,i})}^{t(v_{CE}=2\%V_{CC})} i_{C,i} \cdot v_{CE}\,dt \quad (7)$$

Table III shows the switching characteristics of individual power modules obtained from the measurements and the pair imbalance ratio calculated based on them. ΔI_C and ΔE_{on} are calculated for power module A-power module B, respectively.

Table III: Switching Characteristics of Each Power Module and Pair Imbalance Ratio in Turn-on Measurements

	Power Module A		Power Module B		Imbalance Ratio	
Pair No.	$I_{C,1}$	$E_{on,1}$	$I_{C,2}$	$E_{on,2}$	x_{I_C}= 0.5 $\Delta I_C/I_{C,avg}$	$x_{E_{on}}$= 0.5 $\Delta E_{on}/E_{on,avg}$
1	564 A	0.697 J	556 A	0.682 J	0.7 %	1.1 %
2	586 A	0.774 J	517 A	0.708 J	6.3 %	4.5 %
3	570 A	0.849 J	514 A	0.822 J	5.2 %	1.6 %
4	527 A	0.693 J	590 A	0.751 J	-5.7 %	-4.0 %
5	606 A	0.769 J	511 A	0.680 J	8.5 %	6.1 %
6	531 A	0.759 J	559 A	0.785 J	-2.6 %	-1.7 %
7	548 A	0.770 J	549 A	0.770 J	-0.1 %	0.0 %
8	499 A	0.752 J	593 A	0.800 J	-8.7 %	-3.1 %
9	546 A	0.780 J	543 A	0.772 J	0.3 %	0.5 %
10	519 A	0.844 J	574 A	0.872 J	-5.0 %	-1.6 %

As previously, multiple linear regression analysis has been performed on the measured switching results. For the turn-on collector current imbalance, correlation on ΔV_{EC} and $\Delta V_{GE(th)}$ was evident. The regression equation can be defined as (8).

$$x_{I_C\_typ} = 0.5\,\frac{\Delta I_C}{I_{Cavg}} \approx -0.09\ \mathrm{V}^{-1} \cdot \Delta V_{EC} - 0.09\ \mathrm{V}^{-1} \cdot \Delta V_{GE(th)} \qquad \text{with } R^2 = 0.992 \qquad (8)$$

Figures 11 and 12 shows the imbalance ratios of the turn-on collector current $0.5\ \Delta I_C/I_{C,avg}=(I_{C,1}-I_{C,2})/(I_{C,1}+I_{C,2})$ that depend on the emitter-collector forward voltage differences $\Delta V_{EC}=V_{EC,1}-V_{EC,2}$ and the gate-emitter threshold voltage differences $\Delta V_{GE(th)}=V_{GE(th),1}-V_{GE(th),2}$, respectively.
The equation for the 99% prediction interval shown in Figure 13 is defined as (9).

$$x_{I_C\_PI=99\%} = x_{I_C\_typ} \pm 3.83 \times \sqrt{2.93 \times 10^{-5} \times \left(1 + \frac{1}{10} + \frac{(\Delta V_{EC} - 0.022\ V)^2}{0.187\ V^2} + \frac{\left(\Delta V_{GE(th)} - 0.012\ V\right)^2}{2.331\ V^2}\right)} \qquad (9)$$

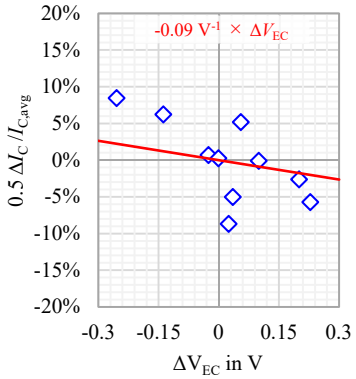

Fig. 11: Imbalance ratio of turn-on collector current (x_{I_C}) in dependence of ΔV_{EC}

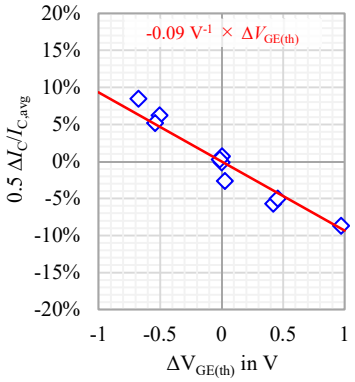

Fig. 12: Imbalance ratio of turn-on collector current (x_{I_C}) in dependence of $\Delta V_{GE(th)}$

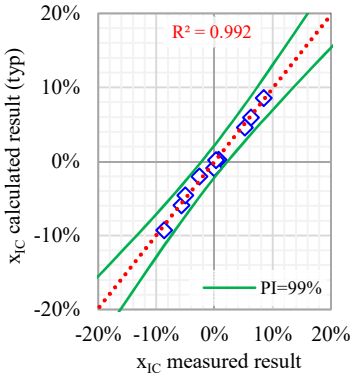

Fig. 13: Correlation of x_{I_C} between calculated and measured results

The imbalance ratio of turn-on energy is also correlated to ΔV_{EC} and $\Delta V_{GE(th)}$, and the regression equation is defined as (10).

$$x_{E_{on}\_typ} = 0.5\,\frac{\Delta E_{on}}{E_{on,avg}} \approx -0.12\ \mathrm{V}^{-1} \cdot \Delta V_{EC} - 0.04\ \mathrm{V}^{-1} \cdot \Delta V_{GE(th)} + 0.007 \qquad \text{with } R^2 = 0.991 \qquad (10)$$

Figures 14 and 15 shows the imbalance ratios of the turn-on energy $0.5\ \Delta E_{on}/E_{on,avg}=(E_{on,1}-E_{on,2})/(E_{on,1}+E_{on,2})$ that depend on the emitter-collector forward voltage differences $\Delta V_{EC}=V_{EC,1}-V_{EC,2}$ and the gate-emitter threshold voltage differences $\Delta V_{GE(th)}=V_{GE(th),1}-V_{GE(th),2}$, respectively. Figure 14 includes the intercept of regression equation (10).
The equation for the 99% prediction interval shown in Figure 16 is defined as (11).

$$x_{E_{on}\_PI=99\%} = x_{E_{on}\_typ} \pm 4.03 \times \sqrt{1.19 \times 10^{-5} \times \left(1 + \frac{1}{10} + \frac{(\Delta V_{EC} - 0.022\ V)^2}{0.187\ V^2} + \frac{\left(\Delta V_{GE(th)} - 0.012\ V\right)^2}{2.331\ V^2}\right)} \qquad (11)$$

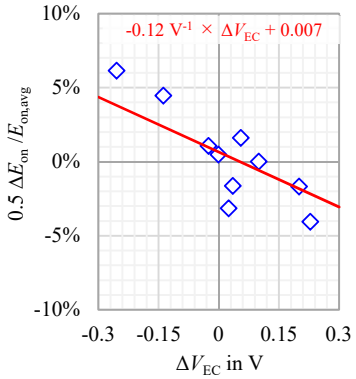

Fig. 14: Imbalance ratio of turn-on switching energy ($x_{E_{on}}$) in dependence of ΔV_{EC}

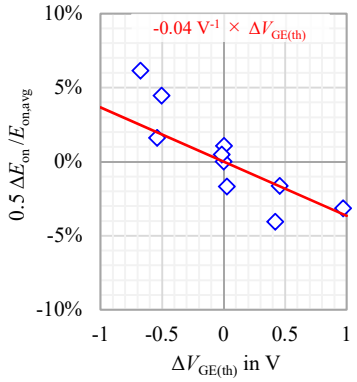

Fig. 15: Imbalance ratio of turn-on switching energy ($x_{E_{on}}$) in dependence of $\Delta V_{GE(th)}$

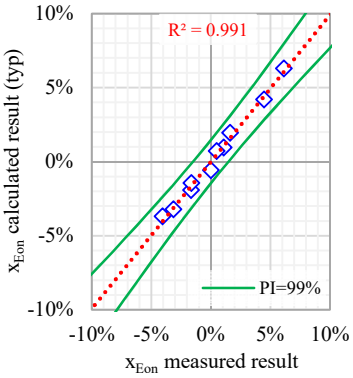

Fig. 16: Correlation of $x_{E_{on}}$ between calculated and measured results

Regarding Diode Reverse-recovery Switching

The reverse-recovery emitter current $I_{E,i}$ (cf. Figure 5) and reverse-recovery energy $E_{rec,i}$ (12) has been evaluated.

$$E_{\mathrm{rec},i} = -\int_{t(v_{EC}=2\%V_{cc})}^{t(i_{E,i}=-2\%I_{E,i})} i_{E,i} \cdot v_{CE}\, \mathrm{d}t \tag{12}$$

Table IV shows the switching characteristics of individual power modules obtained from the measurements and the pair imbalance ratio calculated based on them. ΔI_E and ΔE_{rec} are calculated for power module A-power module B, respectively.

Table IV: Switching Characteristics of Each Power Module and Pair Imbalance Ratio in Reverse-recovery Measurements

	Power Module A		Power Module B		Imbalance Ratio	
Pair No.	$I_{E,1}$	$E_{rec,1}$	$I_{E,2}$	$E_{rec,2}$	x_{I_E}= 0.5 $\Delta I_E/I_{E,avg}$	$x_{E_{rec}}$= 0.5 $\Delta E_{rec}/E_{rec,avg}$
1	453 A	0.913 J	450 A	0.943 J	0.2 %	-1.6 %
2	472 A	0.906 J	417 A	0.835 J	6.2 %	4.1 %
3	432 A	0.740 J	461 A	0.841 J	-3.3 %	-6.4 %
4	404 A	0.767 J	486 A	0.983 J	-9.2 %	-12.4 %
5	502 A	0.945 J	393 A	0.760 J	12.2 %	10.8 %
6	418 A	0.733 J	467 A	0.930 J	-5.6 %	-11.9 %
7	435 A	0.735 J	449 A	0.851 J	-1.6 %	-7.3 %
8	448 A	0.797 J	436 A	0.835 J	1.4 %	-2.3 %
9	452 A	0.782 J	460 A	0.823 J	-0.9 %	-2.6 %
10	441 A	0.780 J	459 A	0.852 J	-2.0 %	-4.4 %

As so far, multiple linear regression analysis has been performed on the measured switching results. For the reverse-recovery emitter current imbalance, correlation on only ΔV_{EC} is evident. The regression equation can be defined as (13).

$$x_{I_{E\_typ}} = 0.5\,\frac{\Delta I_E}{I_{Eavg}} \approx -0.39\ \mathrm{V}^{-1} \cdot \Delta V_{EC} \qquad \text{with } R^2 = 0.923 \tag{13}$$

Figures 17 shows the imbalance ratios of the reverse-recovery emitter current 0.5 $\Delta I_E/I_{E,avg}$=($I_{E,1}$-$I_{E,2}$)/($I_{E,1}$+$I_{E,2}$) that depend on the emitter-collector forward voltage differences ΔV_{EC}=$V_{EC,1}$-$V_{EC,2}$. The equation for the 99% prediction interval shown in Figure 18 is defined as (14).

$$x_{I_{E\_PI=99\%}} = x_{I_{E\_typ}} \pm 3.69 \times \sqrt{2.76 \times 10^{-4} \times \left(1 + \frac{1}{10} + \frac{(\Delta V_{EC} - 0.022\ V)^2}{0.187\ V^2}\right)} \quad (14)$$

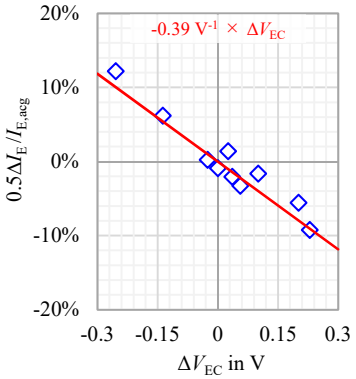

Fig. 17: Imbalance ratio of reverse-recovery emitter current (x_{I_E}) in dependence of ΔV_{EC}

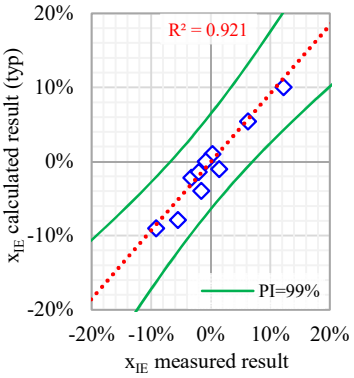

Fig. 18: Correlation of x_{I_E} between calculated and measured results

The imbalance ratio of reverse-recovery energy is also correlated to only ΔV_{EC}, and the regression equation is defined as (15).

$$x_{E_{rec\_typ}} = 0.5\ \frac{\Delta E_{rec}}{E_{rec,avg}} \approx -0.48\ V^{-1} \cdot \Delta V_{EC} - 0.023 \qquad \text{with } R^2 = 0.987 \quad (15)$$

Figures 19 shows the imbalance ratios of the reverse-recovery energy $0.5\ \Delta E_{rec}/E_{rec,avg}=(E_{rec,1}-E_{rec,2})/(E_{rec,1}+E_{rec,2})$ that depend on the emitter-collector forward voltage differences $\Delta V_{EC}=V_{EC,1}-V_{EC,2}$. Figure 19 includes the intercept of regression equation (15).
The equation for the 99% prediction interval shown in Figure 20 is defined as (16).

$$x_{E_{rec\_PI=99\%}} = x_{E_{rec\_typ}} + 3.83 \times \sqrt{7.34 \times 10^{-5} \times \left(1 + \frac{1}{10} + \frac{(\Delta V_{EC} - 0.022\ V)^2}{0.187\ V^2}\right)} \quad (16)$$

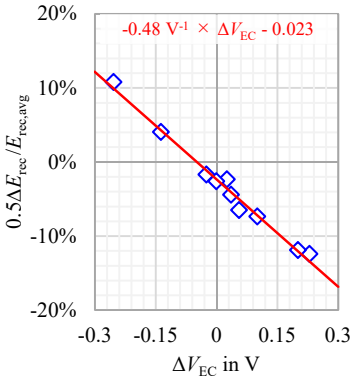

Fig. 19: Imbalance ratio of reverse-recovery switching energy ($x_{E_{rec}}$) in dependence of ΔV_{EC}

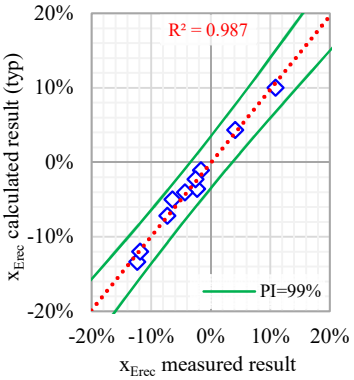

Fig. 20: Correlation of $x_{E_{rec}}$ between calculated and measured results

Analysis of Required Parameter Derating Based on the Module Parameters

The regression equations defined in the previous chapters to define the current and energies imbalance ratios are used to calculate the derating ratio required in case of parallel connection of more than two modules. For this, it will be assumed that one of the paralleled modules has a minimum characteristic (resulting in maximum switching energy or current) while all other modules have the maximum

characteristics (leading to minimum switching energy or current). As an example, the formula for the turn-off collector current derating ratio is shown as (17).

$$\frac{I_{\mathrm{C,max}}}{I_{\mathrm{C,avg}}} - 1 = \frac{I_{\mathrm{C,max}}}{\left((n-1)I_{\mathrm{C,min}} + I_{\mathrm{C,max}}\right)/n} - 1 = \frac{n \cdot I_{\mathrm{C,max}}}{\left((n-1)\frac{1-x}{1+x}I_{\mathrm{C,max}} + I_{\mathrm{C,max}}\right)} - 1 = \frac{n}{\left((n-1)\frac{1-x}{1+x} + 1\right)} - 1 \tag{17}$$

The parameter n is in this formula the number of paralleled modules. The parameter x is the identified imbalance ratio from this measurement. As a result, the derating dependency on the power-module parameters can be defined as shown in Figure 21. The figure shows that the prediction intervals, as determined by the regression analysis are also very helpful with respect to derating ratios in case of parallel connection of more than two modules.

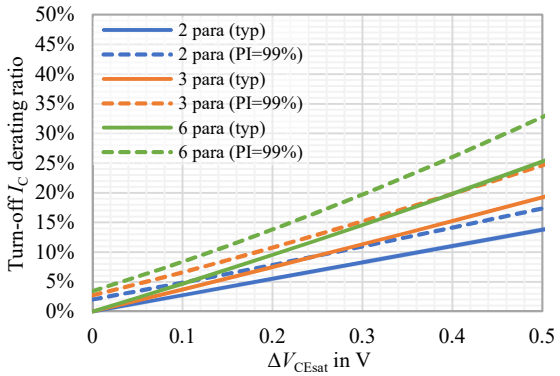

Fig. 21: Turn-off I_C derating ratio vs. ΔV_{CEsat}

As above, the derating ratios for other switching characteristics have been also calculated and defined as shown in Figure 22 ~ Figure 29 for each correlated power module parameter.

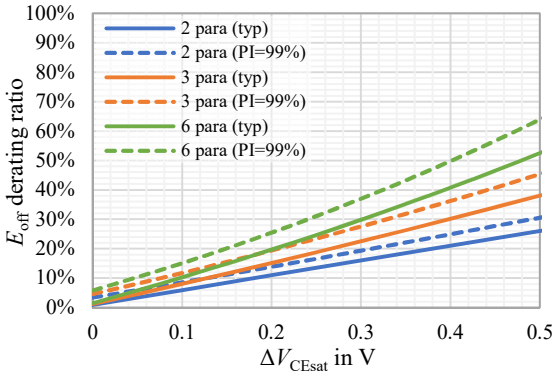

Fig. 22: E_{off} derating ratio vs. ΔV_{CEsat}

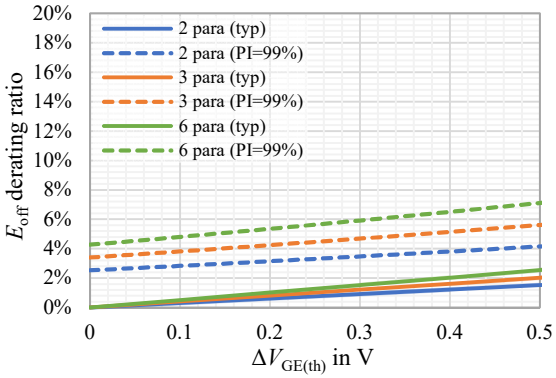

Fig. 23: E_{off} derating ratio vs. $\Delta V_{GE(th)}$

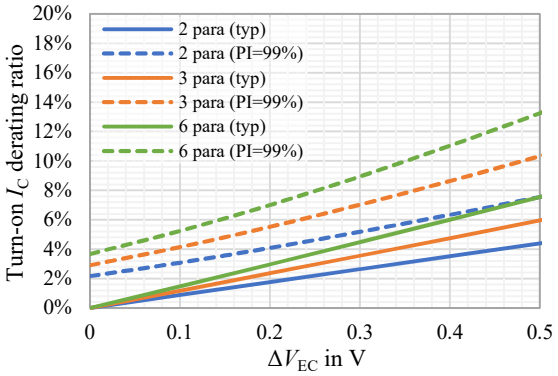

Fig. 24: Turn-on I_C derating ratio vs. ΔV_{EC}

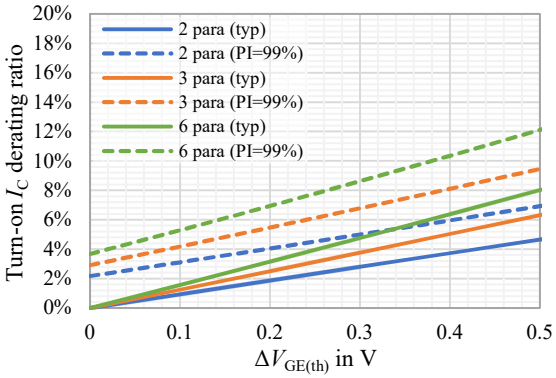

Fig. 25: Turn-on I_C derating ratio vs. $\Delta V_{GE(th)}$

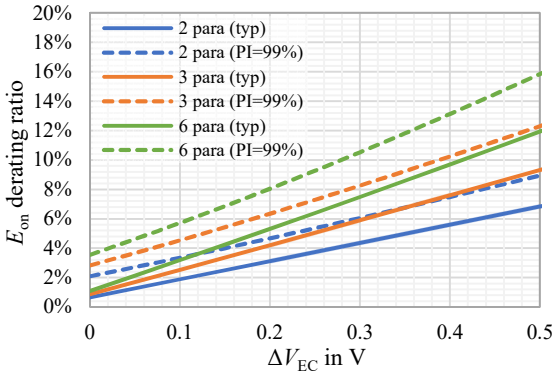

Fig. 26: E_{on} derating ratio vs. ΔV_{EC}

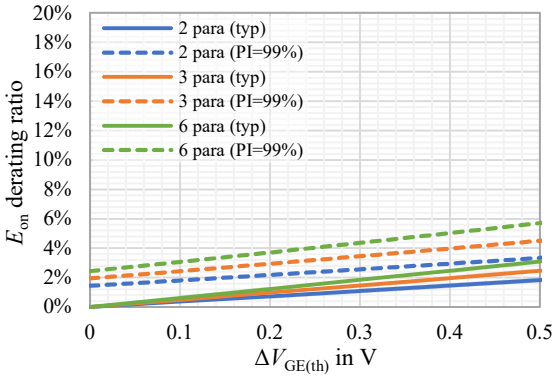

Fig. 27: E_{on} derating ratio vs. $\Delta V_{GE(th)}$

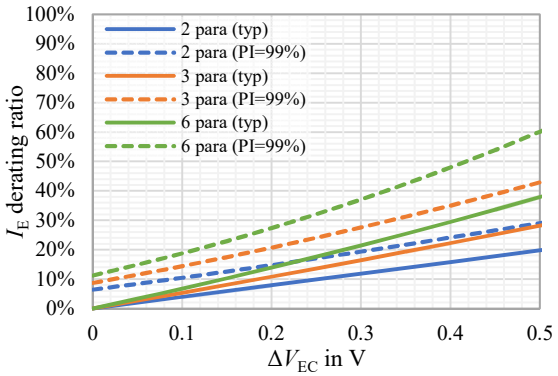

Fig. 28: I_E derating ratio vs. ΔV_{EC}

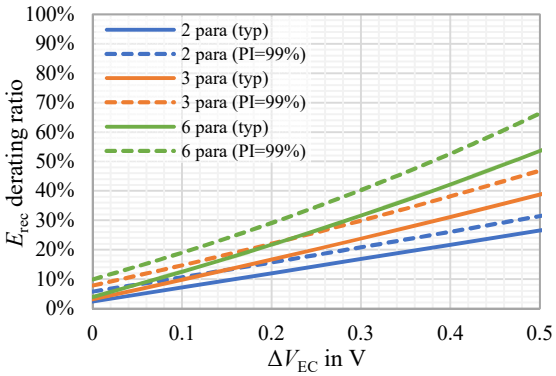

Fig. 29: E_{rec} derating ratio vs. ΔV_{EC}

Conclusion

This paper has shown a methodology to evaluate the influence of IGBT power module parameters on switching characteristics of power modules connected in parallel. For this purpose, the switching waveforms of ten different pairs of IGBT power modules connected in parallel have been analyzed. Using multiple linear regression on the measured data identifies correlation between power-module parameters and switching characteristics as current imbalance and inhomogeneous switching energies. The methodology allows the definition of pairing criteria for IGBT power modules in parallel connection. Moreover, the results can also be used to calculate the derating for two or more power modules in parallel.

In actual applications, the imbalance in current sharing causes the temperature of devices with high current flow to rise. However, if forward voltage characteristics of IGBTs and diodes have a positive temperature dependence, the current sharing imbalance will decrease. Hence, actual derating, including switching losses, might be lower compared to the results calculated here.

References

[1] T. Wiik, „D1.2, New generation power semiconductor, Common specification for traction and market analysis, technology roadmap, and value cost prediction," Roll2Rail, H2020 - 636032, 2016.

[2] J. Weigel, J. Boehmer, A. Nagel und R. Kleffel, „Paralleling high power dual modules: A challenge for application engineers and power device manufacturers," in 2017 19th European Conference on Power Electronics and Applications (EPE'17 ECCE Europe), Warsaw, Poland, 2017.

[3] N. Chen, F. Chimento und e. al, „Dynamic Characterization of Parallel-Connected High-Power IGBT Modules," IEEE Trans. on Ind. Appl., Bd. 51, Nr. 1, pp. 539-546, 2015.

[4] J. Weigel, J. Boehme und e. al, „Paralleling of High Power Dual Modules: Standard Building Block Design for Evaluation of Module Related Current Mismatch," in 2018 20th European Conference on Power Electronics and Applications (EPE'18 ECCE Europe), Riga, Latvia, 2018.

[5] A. Nagel, J. Weigel, et. al., „Paralleling reference setup,“ Shift2Rail, Pinta, H2020 - 730668, 2019.

[6] Mitsubishi Electric Corporation, Press Release No. 3104, Mitsubishi Electric to Launch LV100-type X-Series HVIGBT Modules, Tokyo, 2017.

[7] N. Inagaki, Mathematical Statistics, (in Japanese), Japan: Shokabo Co. Ltd., 2009, pp. 196-205.